ACS chemical biology

Articles

pubs.acs.org/acschemicalbiology

Mechanism of Allosteric Inhibition of the Enzyme IspD by Three Different Classes of Ligands

Anatol Schwab,[†] Boris Illarionov,[‡] Annika Frank,[§] Andrea Kunfermann,[§] Michael Seet,[†] Adelbert Bacher,[§] Matthias C. Witschel,*[,∥] Markus Fischer,*[,‡] Michael Groll,*[,§] and François Diederich*[,†]

[†]Laboratorium für Organische Chemie, ETH Zurich, Vladimir-Prelog-Weg 3, 8093 Zurich, Switzerland

[‡]Hamburg School of Food Science, Universität Hamburg Grindelallee 117, 20146 Hamburg, Germany

[§]Center for Integrated Protein Science Munich, Lehrstuhl für Biochemie, Technische Universität München, Lichtenbergstrasse 4, 85748 Garching, Germany

[∥]BASF SE, Carl-Bosch-Strasse 38, 67056 Ludwigshafen, Germany

Supporting Information

ABSTRACT: Enzymes of the nonmevalonate pathway of isoprenoid biosynthesis are attractive targets for the development of herbicides and drugs against infectious diseases. While this pathway is essential for many pathogens and plants, mammals do not depend on it for the synthesis of isoprenoids. IspD, the third enzyme of the nonmevalonate pathway, is unique in that it has an allosteric regulatory site. We elucidated the binding mode of phenylisoxazoles, a new class of allosteric inhibitors. Allosteric inhibition is effected by large conformational changes of a loop region proximal to the active site. We investigated the different roles of residues in this loop by mutation studies and identified repulsive interactions with Asp291 and Asp292 to be responsible for inhibition. Crystallographic data and the response of mutant enzymes to three different classes of allosteric inhibitors provide an in-depth understanding of the allosteric mechanism. The obtained mutant enzymes show selective resistance to allosteric inhibitors and provide conceptually valuable information for future engineering of herbicide-resistant crops. We found that the isoprenoid precursors IPP and DMAPP are natural inhibitors of *Arabidopsis thaliana* IspD; however, they do not seem to bind to the allosteric site.

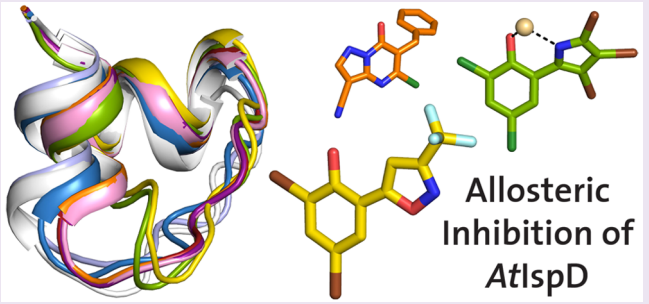

There is an urgent need for new herbicidal modes of action (MOAs) due to the increasing resistance developing against the established ones in key weeds. For these new MOAs, it would be highly desirable to start developing concepts for herbicide-tolerant crops as early as possible. Due to extensive deregulation studies and the long time required to breed seeds for market introduction, the current marketing time for a new herbicide-tolerant trait is even longer than for the development of a new active ingredient.[1]

Inhibitors of the enzymes in the nonmevalonate pathway of isoprenoid biosynthesis (Scheme 1A) are attractive targets, as this pathway is essential to many pathogens and plants but absent in humans.[2−5] With early structural information on two classes of inhibitors binding to an allosteric pocket of the third enzyme IspD from *Arabidopsis thaliana* (*At*) of the pathway in hand (**1**−**3**, Scheme 1B), we had the opportunity to examine rational approaches that avoid the inhibitory effects of their interactions with the allosteric pocket.[6−8] As the latter leads to the closure of the IspD active site, it could be possible to modify the enzyme in a way that inhibitor binding does not result in this effect, thereby retaining the enzymatic activity. Such an approach might allow the development of crops that are insensitive to the herbicide and potentially provide higher levels of tolerance and enzymatic activity than the active site modifications that are predominantly employed for the design of target-based herbicide tolerance in crops to date.[9]

Here, we report the first member of a third, new class of allosteric *At*IspD inhibitors, phenylisoxazole **4** (Scheme 1B), and elucidate its binding mode by cocrystal structure analysis. Derivatives **5**−**7** provide an informative structure−activity relationship (SAR) for the new class and allow estimation of the energetic contributions of the individual binding interactions (Table 1). An ensemble of crystallographic data on the complexes of the three classes of allosteric ligands with native and mutant *At*IspD enzymes, complemented by kinetic profiling and binding studies, provides a refined model of the allosteric mechanism for substrate inhibition and particularly highlights contributions from an allosteric site loop to this mechanism.[10−12] Downstream metabolites IPP and DMAPP of the pathway (Scheme 1B) were identified as natural inhibitors

Received: January 3, 2017
Accepted: June 22, 2017

DOI: 10.1021/acschembio.7b00004
ACS Chem. Biol. XXXX, XXX, XXX−XXX

Scheme 1. (A) Function of IspD in the Non-Mevalonate Pathway of Isoprenoid Synthesis[2−5,a] and (B) Inhibitors of *At*IspD

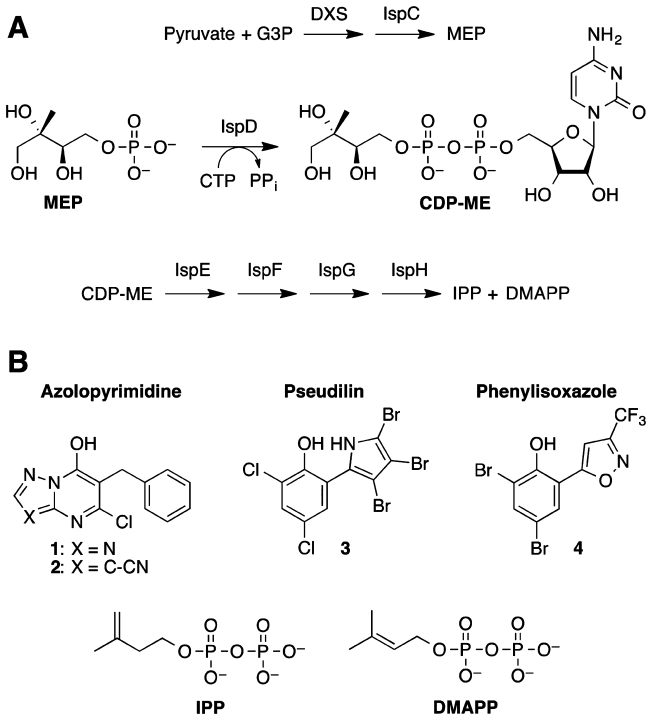

[a]IspD: 4-diphosphocytidyl-2*C*-methyl-D-erythritol synthase (EC 2.7.7.60). MEP: 2*C*-methyl-D-erythritol 4-phosphate. CDP-ME: 4-diphosphocytidyl-2C-methyl-D-erythritol. Full names and EC numbers of all enzymes are listed in the abbreviations section.

Table 1. Structure−Activity Relationship for Phenylisoxazoles 4−7

Structure	Number	R^1	R^2	*At*IspD IC_{50} [μM]
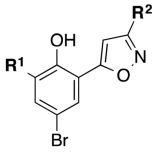	**4**	Br	CF_3	9.3 ± 0.6
	5	Br	H	121 ± 11
	6	H	CF_3	418 ± 75
	7	H	H	> 500

of *At*IspD; however, they do not seem to bind to the allosteric site.

RESULTS AND DISCUSSION

Allosteric and Active Sites in *At*IspD. The active site of *At*IspD comprises subpockets for the methylerythritol, phosphate, ribose, and cytosine moieties of the substrates 2*C*-methyl-D-erythritol 4-phosphate (MEP) and CTP (Scheme 1A). The allosteric pocket, which opens up upon binding the previously reported allosteric inhibitors **1**−**3**[7,8,13] and the new phenylisoxazol ligand **4** (Figure 1) is in close proximity, 6−8 Å away from the methylerithritol subpocket. This binding pocket is not developed in the ligand-free state, and conformational changes induced by its formation mediate the allosteric inhibition (see below). Figure 1 shows the complex of the new allosteric inhibitor **4** overlaid with a product-bound crystal structure of IspD from *Escherichia coli* (*Ec*).[14−16] The extension of the allosteric pocket and the nature of the protein-inhibitor

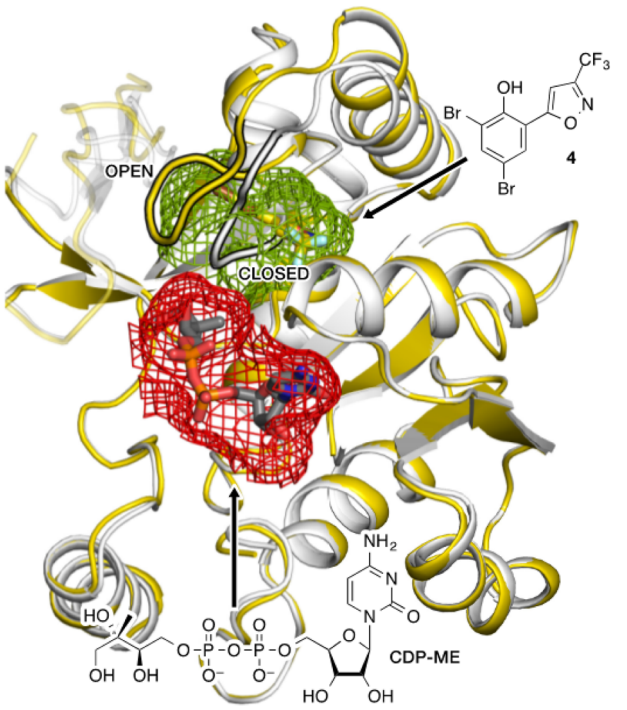

Figure 1. Allosteric and active site of *At*IspD. The overlay of *apo* *At*IspD (white, PDB ID: 4NAI, 1.5 Å) and of **4**-bound *At*IspD (yellow, PDB ID: 5MRM, 1.8 Å) shows the adjacency of the two sites.[8] The green mesh surface spans the volume of the allosteric site of **4**-bound *At*IspD; the red mesh surface, the active site of *apo* *At*IspD. CDP-ME (gray) was overlaid from a product-bound crystal structure of *Ec*IspD (PDB ID: 1INI, 1.8 Å).[14] Allosteric site loop regions in the *apo* (closed) and inhibitor **4**-bound (open) conformations are outlined in black.[15,16] For a view of the dimer, see Supporting Information, Figure S1.

interactions differ substantially between the three classes of ligands **1**−**4** (Figure 2). All ligands are present as anionic species at physiological pH, with a measured pK_a value of 3.9 (**1**)[7] and calculated values of 6.3 (OH) and 9.0 (NH) for **3** and 5.9 (OH) for **4**.[17] They all most probably bind in their anionic form. Azolopyrimidines **1** and **2** interact through a hydrogen-bonding network, and a tight hydrophobic pocket accommodates the phenyl ring (Figure 2A).[7,18] Pseudilin **3**, a member of a class of marine natural products,[19−23] undergoes distinct halogen bonding[24−26] in an overall larger pocket (Figure 2B), and inhibitory activity is enhanced by coordinative binding, if a divalent cation, such as Cd^{2+} (or Ca^{2+}, Cu^{2+}, Zn^{2+}), is supplied (Table 2).[8]

Metal-Ion-Free Allosteric Inhibition by the Phenylisoxazole Ligand 4. In our effort to develop inhibitors of *At*IspD that do not bind *via* metal interaction, the phenylisoxazole ligand **4** was identified from a screening set selected for pseudilin structure similarity. Inhibition occurs at a similar strength to that of the pseudilin ligands,[8] with an IC_{50} (*At*IspD) = 9.3 μm, and is unaffected by the addition of Cd^{2+} (Table 2).[27] As for **1**, potent postemergence herbicidal activity (+++) of **4** was observed for two of the four tested agronomically relevant weeds, which supports favorable physicochemical properties and permeability across plant membranes (Supporting Information, Table S1), even though based on these studies additional modes of action cannot be ruled out and warrant further advanced experiments. Binding to the allosteric site in the absence of a metal ion was confirmed by a cocrystal

DOI: 10.1021/acschembio.7b00004
ACS Chem. Biol. XXXX, XXX, XXX−XXX

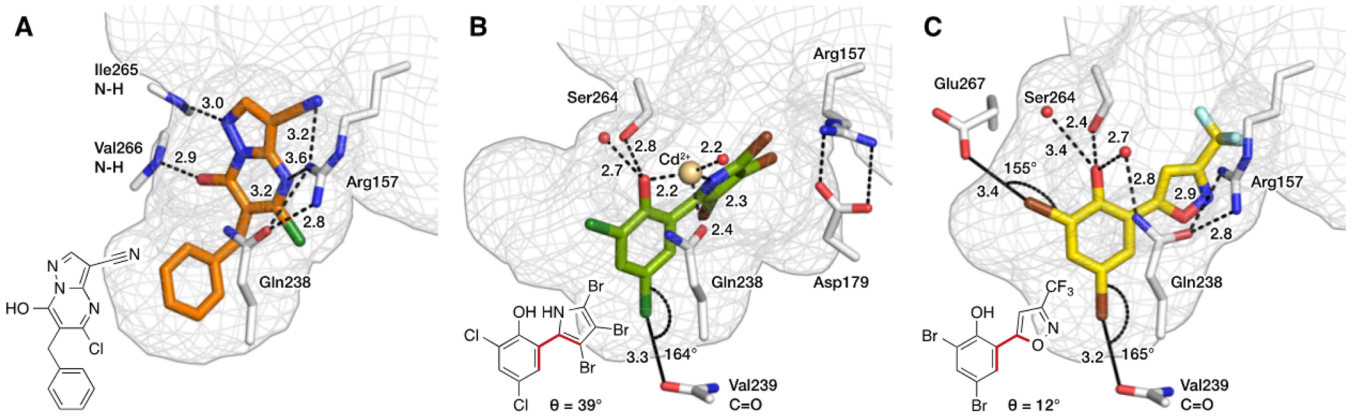

Figure 2. Binding modes of inhibitors to the allosteric site of *At*IspD. (A) Azolopyrimidine **2** (orange) interacts through a hydrogen bonding network and filling of a tight hydrophobic pocket (PDB ID: 2YC5, 1.6 Å).[7] (B) Pseudilin **3** (green) through halogen and hydrogen bonding and ion coordination (PDB ID: 4NAL, 1.8 Å).[8] (C) Binding of phenylisoxazole **4** (yellow) through halogen and hydrogen bonding (PDB ID: 5MRM, 1.8 Å). Phenols of **1**–**4** are acidic, and the ligands are most probably bound in an anionic form. The outlined mesh surface spans the volume of the allosteric site, which is dependent on the bound inhibitor. Atom coloring: Br brown, Cd yellow, Cl green, F cyan, N blue, O red; interacting amino acids are displayed in white. Distances are given in Å; for biaryl systems, the dihedral angle is given.

Table 2. Characterization of *At*IspD Resistance Mutants and Selective Impact of Mutations on Different Ligand Classes

*At*IspD	k_{cat} [min^{-1}]	K_S [μM] (CTP)	K_S [μM] (MEP)	IC_{50} [μM] (**1**)	IC_{50} [μM] (**2**)	IC_{50} [μM] (**3**)	IC_{50} [μM] (**3**) + 40 μM Cd^{2+}	IC_{50} [μM] (**4**)	IC_{50} [μM] (**4**) + 40 μM Cd^{2+}
Wild type	13 ± 1	77 ± 18	123 ± 8	0.18 ± 0.02	0.029 ± 0.002	40 ± 4	5.8 ± 0.7	9.3 ± 0.6	9.2 ± 1.0
E258A	3.9 ± 0.3	63 ± 3	169 ± 32	2.0 ± 0.1	3.0 ± 0.3		5.7 ± 0.3	13 ± 1	
D262A	0.78 ± 0.05	427 ± 27	330 ± 20	149 ± 9	23 ± 1		247 ± 9	234 ± 107	

structure (1.8 Å resolution, PDB ID 5MRM, Figures 1 and 2C; electron density around **4** in Figure S2 in the Supporting Information (SI)). The chemical structure of **4** shares the 2,4-dibromophenol motif with the pseudilin class while the tribromopyrrole is replaced by the aprotic 3-trifluoromethylisoxazole moiety (Scheme 1B). In the bound state, the biaryl system of **4** assumes an almost flat conformation with a smaller dihedral angle (12°) than observed for pseudilin **3** (39°; Figure 2B,C). The isoxazole O atom faces away from the phenol, avoiding repulsive interactions with the most probable anionic phenoxide.

Binding is mediated by a halogen bond to the C═O of Val239 (d(O···Br) = 3.2 Å, ∠(C–Br···O) = 165°) in analogy to the similar interaction in the pseudilin complexes. A second halogen bond is established to the side-chain C═O of Glu267.[28] The phenoxide O^- atom engages in a H-bonding network with the HO side chain of Ser264 (d(O···O) = 2.4 Å) and a water molecule (d(O···O) = 2.7 Å); the latter also forms a bridge to the NH_2 group of Gln238 (d(O···N) = 2.8 Å). The side-chain C═O of Gln238 interacts with two N atoms of the guanidinium moiety of Arg157 (d(O···N) = 2.8 and 2.9 Å, respectively); the geometry of these two amino acids is similar to the one observed in the complex of azolopyrimidine **2** (Figure 2A,C).

This contrasts the pseudilin-bound state where the side-chain C═O of Gln238 coordinates to the Cd^{2+} ion and Arg157 interacts with Asp179 at the substrate ribose site (Figure 2B vs A, C). Despite the similar chemical structure, this finding implies a different mode of inhibition and separates phenylisoxazole **4** from the pseudilin ligand class.[8]

The dibromophenol ring in **4** is sandwiched between the side chains of Val266 and Gln238, which form a cleft of 7.0 Å width, ideal for the intercalation of an aromatic ring.[29,30] The valine methyl groups undergo C–H···π interactions, and the carboxamide side chain of Gln238 stacks in a parallel-shifted way on the aromatic ring (Figure 3).[31] The CF_3 group is in a truly fluorophilic environment and undergoes a short, H-bond-like interaction with one of the guanidinium N–H's of Arg157 (d(F···N) = 3.0 Å).[32,33]

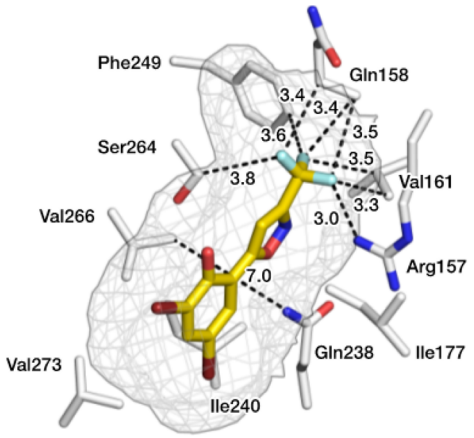

Figure 3. Interactions of **4** with the hydrophobic allosteric pocket of *At*IspD (PDB ID: 5MRM, 1.8 Å). The outlined mesh surface spans the volume of the allosteric site. Atom coloring: Br brown, F cyan, N blue, O red; interacting amino acids are displayed in white. Distances are given in Å.

Numerous lipophilic interactions, with C···F distances between 3.8 and 3.3 Å, are established by the CF_3 group and alkyl moieties in the surrounding side chains of Ser264, Arg157, Val161, and Gln158, as well as with a C_{sp2}–H of Phe249 (Figure 3).

The SAR for phenylisoxazoles **4**–**7** allowed quantification of the effects of the different binding interactions of lead structure

DOI: 10.1021/acschembio.7b00004
ACS Chem. Biol. XXXX, XXX, XXX–XXX

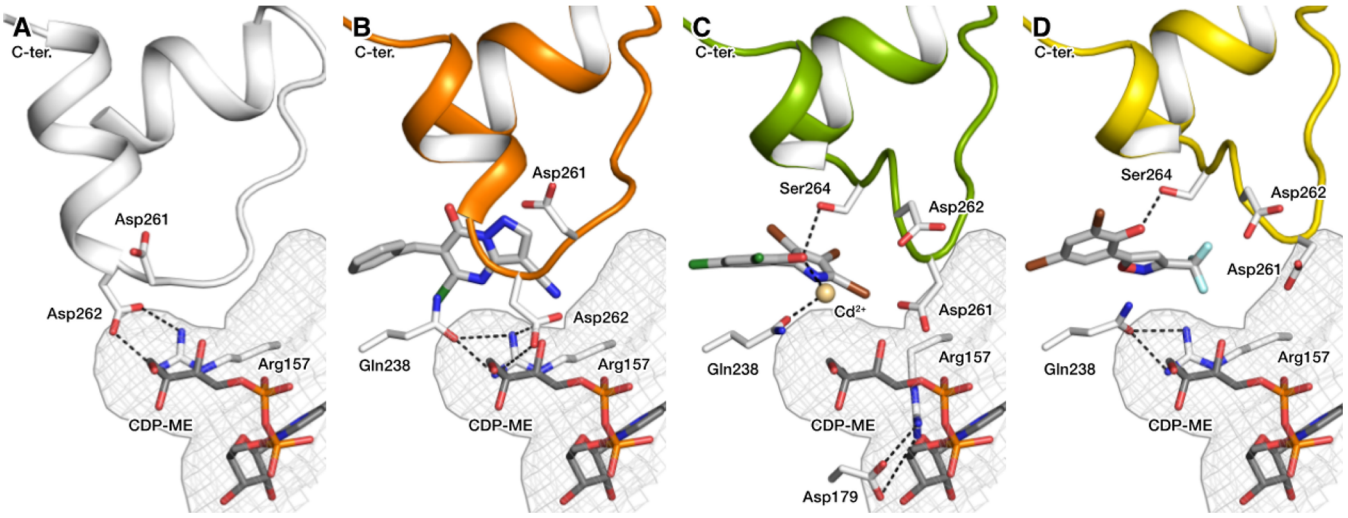

Figure 4. Comparison of loop conformations at the allosteric site of wild type *At*IspD upon ligand binding. Gradual unwinding of the helix at the C-terminus of the loop region between Gly256 and Asp262 from A to D in response to ligand binding. CDP-ME (gray) was overlaid from a product-bound crystal structure of *Ec*IspD (PDB ID: 1INI, 1.8 Å).[14] The mesh surface spans the volume of the active site. (A) Allosteric site loop of *apo* *At*IspD (white, PDB ID: 4NAI, 1.5 Å).[8] (B) Allosteric site loop of azolopyrimidine **2**-bound *At*IspD (orange, PDB ID: 2YC5, 1.6 Å).[7] Asp262 protrudes into the MEP substrate pocket. (C) Allosteric site loop of pseudilin **3**-bound *At*IspD (green, PDB ID: 4NAL, 1.8 Å).[8] Asp261 is oriented toward the MEP substrate pocket, and the ion pair between Arg157 and Asp179 fills the space of the ribose binding site. (D) Allosteric site loop of phenylisoxazole **4**-bound *At*IspD (yellow, PDB ID: 5MRM, 1.8 Å). Largest observed loop movement, with Asp261 oriented toward the phosphate binding site at a 5.5 Å distance to the phosphate of CDP-ME. Atom coloring: Br brown, Cd yellow, Cl green, F cyan, N blue, O red, P orange; interacting amino acids are displayed in white.

4 with the protein. Replacement of the CF_3 group in **4** by hydrogen (**5**) decreases binding by a factor of 13 (Table 1) and specifies a predictive value for the contribution of CF_3 groups in a favorable environment.[33] Substitution of the bromine *ortho* to the phenoxide by hydrogen (**6**) leads to a 45-fold loss in potency which can be attributed to the loss of the strong halogen bond to Glu267 and a decreased acidification of the phenol.[26,34−37] The combined replacement of the *ortho* bromine and the CF_3 group by hydrogen renders phenylisoxazole **7** inactive within the range of the assay, marking the limits of the phenylisoxazole ligand class.

Allosteric Site Loop of *At*IspD. A comparison of *apo* and ligand-bound crystal structures reveals conformational changes of the loop between the two α-helices between Gly256 and Asp262 upon allosteric binding. The three classes of allosteric ligands displace the loop to different extents, and their cocrystal structures provide remarkable snapshots of its movement. A gradual unwinding of the α-helix at the C-terminal end of the loop and an increasing displacement are observed going from the azolopyrimidine- to the pseudilin- and to the phenylisoxazole-bound state (Figure 4A−D). The largest loop movement is observed for bound phenylisoxazole **4**, which displaces the C_α of Asp262 by 10 Å and that of Asp261 by 7 Å, compared to the *apo* structure. As the cocrystal structure of *At*IspD in complex with **4** shares similar conformations of key amino acids to those seen in both the azolopyrimidine- and pseudilin-bound states, it is possible to infer a common mechanism of inhibition.

In the *apo* state, the side chains of Asp262 and Arg157 undergo the well-documented linear ion pairing with formation of two ionic H bonds (Figure 4A).[38] Upon azolopyrimidine binding, this ion-pairing interaction is disrupted, and the ionic termini of the two side chain termini adopt a parallel-stacked orientation at a close distance of 3.8 Å (between the two planes, Figure 4B). The Arg157 side chain now interacts with the side chain C═O of Gln238. In this loop conformation, the carboxylate of Asp262 protrudes into the MEP pocket, inhibiting the binding of the anionic phosphate substrate.

In the pseudilin-bound state, Asp262 is shifted further and no longer interacts with Arg157 (Figure 4C). In the crystal structure, the interaction between Gln238 and Arg157 is prevented due to coordination of the Cd^{2+} ion to Gln238. As a result, Arg157 rotates away to interact with Asp179, thereby blocking the ribose binding site of CTP. In addition, Asp261 is oriented toward the active site, inducing steric repulsion of the methylerythritol and charge repulsion of the phosphate moiety of the substrate.

The phenylisoxazole-bound state presents features of both the azolopyrimidine- and pseudilin-bound states (Figure 4D). Arg157 remains in its position and interacts with the side-chain C═O of Gln238. At the same time, the open conformation of the loop orients the anionic side chain of Asp261 toward the phosphate pocket, inducing charge−charge repulsion. In this structure-based analysis, Asp261 and Asp262 departing from the allosteric loop are identified as key players of the allosteric mechanism which, with their side chains, interfere with the binding of the anionic substrates MEP and CTP. In the case of the pseudilin ligands, Arg157 additionally interferes with substrate binding, and this might be reflected in the slightly stronger allosteric inhibition of **3** over **4** (IC_{50} = 5.8 vs 9.3 μM).

Mutant *At*IspD Enzymes. The D262A mutant enzyme was generated in order to confirm the role of Asp262 in inhibiting substrate binding and its dependency on the inhibitor class. We expected a lack of inhibition of this mutant by azolopyrimidine ligands, whereas the activity of pseudilin and phenylisoxazole ligands should remain unaffected. The activity of azolopyrimidine **2** against the D262A mutant was reduced 793-fold, while the reduction is only 42-fold for pseudilin **3** (Table 2). The effect of the D262A mutation on azolopyrimidine binding is 19-times higher than on the pseudilin activity.

DOI: 10.1021/acschembio.7b00004
ACS Chem. Biol. XXXX, XXX, XXX−XXX

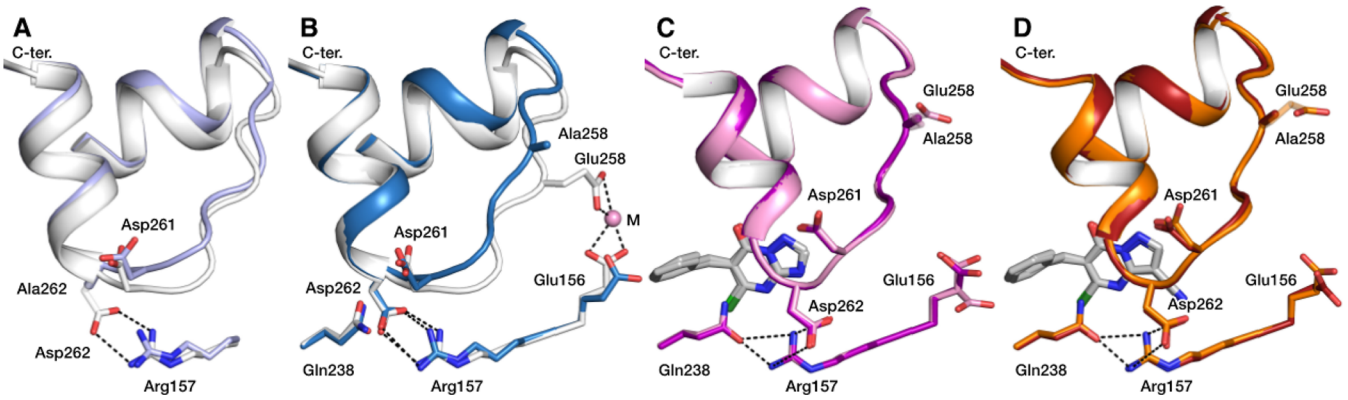

Figure 5. Comparison of loop conformations at the allosteric site of mutated and wild type *At*IspD upon ligand binding. (A) Overlay of *apo* wild type (white, PDB ID: 4NAI, 1.5 Å) and *apo* D262A mutant (light blue, PDB ID: 5MRQ, 2.2 Å).[8] Mutant and wild type show a similar conformation. (B) Overlay of *apo* wild type (white, PDB ID: 4NAI, 1.5 Å) and *apo* E258A mutant (blue, PDB ID: 5MRN, 2.0 Å).[8] Mutant E258A lacks the GLU258−M−GLU156 interaction (M assigned as potassium in PDB ID 4NAI) and shows partial opening of the loop.[8] (C) Overlay of triazolopyrimidine **1** bound to the wild type enzyme (pink, PDB ID: 2YC3, 1.4 Å) and to the E258A mutant (purple, PDB ID: 5MRO, 1.8 Å).[7] (D) Overlay of azolopyrimidine **2** bound to the wild type enzyme (orange, PDB ID: 2YC5, 1.6 Å) and to the E258A mutant (red, PDB ID: 5MRP, 1.9 Å).[7] Atom coloring: Cl green, M pink, N blue, O red.

The *apo* crystal structure of D262A *At*IspD shows high similarity to the structure of the wild type enzyme, and the mutation itself does not affect the conformation of the allosteric site loop (Figure 5A). The measured impact of the mutation on the turnover number therefore likely results from the involvement of Asp262 in substrate interactions rather than from activation of the allosteric mechanism.

A different effect was observed for an alanine mutation of the allosteric loop residue Glu258. In the wild type *apo* state, the metal ion-mediated Glu258−M−Glu156 bridge stabilizes the closed loop conformation (Figure 5B, white). In contrast to the D262A mutant, the *apo* state of E258A shows a more significant movement of the loop toward the azolopyrimidine-bound state (Figure 5B, blue).

Co-crystal structures of E258A *At*IspD with azolopyrimidine **1** and **2** closely resemble the corresponding wild type cocrystal structures, and little effect of the mutation on the ligand-bound state is observed (Figure 5C, D). The reduced enzyme turnover is in accordance with activation of the allosteric mechanism, by loop opening, in the ligand-free state as Glu258 does not interact directly with the substrate. The E258A mutation has a significant impact on the efficacy of azolopyrimidine **1** and **2**, whereas inhibition by pseudilin **3** remains unaffected (Table 2). The reasons for this difference are not apparent from the structural analysis.

For **1**, the mode of inhibition on wild type and E258A *At*IspD was evaluated under variable concentrations of the substrates MEP and CTP. For both enzymes, inhibition uncompetitive with MEP and a mixed inhibition mode toward CTP were found (Table S3, Supporting Information).

Both mutations show a high degree of resistance specific to azolopyrimidine ligands, which is promising for application in herbicide-resistant crops. Natural resistance mutations encountered in herbicide-resistant "superweeds" show similarly reduced enzyme turnover without a loss of fitness of the plants.[39]

Feedback Regulation. To elucidate the biological role of the allosteric site of *At*IspD, we investigated the inhibitory effect of isopentenyl diphosphate (IPP) and dimethylallyl diphosphate (DMAPP), the two products of the MEP pathway (Scheme 1A,B). For both metabolites, inhibition was observed with IC_{50} values of 2.5 mM (DMAPP) and 19 mM (IPP). Thus, reported physiological DMAPP concentrations of up to 3 mM in cottonwood chloroplasts show the potential of biologically relevant inhibition through feedback regulation.[40] While complexes of DMAPP and IPP with other enzymes of the pathway were previously reported, no cocrystals with *At*IspD were obtained.[41] Inhibition by DMAPP was found to be uncompetitive with the allosteric site binder **1** and MEP (Supporting Information, Figures S3−S7) and likely occurs outside of the allosteric pocket and not through an allosteric mechanism. In contrast to CMP for which both stimulation and inhibition of *At*IspD in the mM range was reported, a monotonically increasing inhibitory effect for DMAPP was observed.[42]

Conclusions and Outlook. We identified phenyloxazole **4** as a new lead structure for allosteric inhibition of *At*IspD and analyzed its binding mode based on an X-ray cocrystal structure. Crystallographic data provide a detailed picture of the movement of an allosteric site loop and led to a refined model of the allosteric mechanism in which Asp261 or Asp262 of this loop mediate inhibition of substrate binding. This model was confirmed by mutation studies which yielded mutant enzymes with selective resistance to the azolopyrimidine class of allosteric inhibitors. Downstream metabolites DMAPP and IPP were found to be feedback regulators of *At*IspD independent from the allosteric mechanism. The obtained insight potentially enables the rational design of herbicide-resistant crops and new allosteric inhibitors targeting specific loop conformations.

MATERIALS

Ligands **1**−**3** were obtained as previously reported.[7,8] Ligand **4** (CAS 924871-27-2) was obtained from Interchim.

ASSOCIATED CONTENT

Supporting Information

The Supporting Information is available free of charge on the ACS Publications website at DOI: 10.1021/acschembio.7b00004.

Herbicidal activity of **4**, crystallization of *At*IspD, electron density around ligand **4**, X-ray data collection and

DOI: 10.1021/acschembio.7b00004
ACS Chem. Biol. XXXX, XXX, XXX−XXX

refinement statistics, photometric activity assay, inhibition kinetics of **1**, competition of **1** and MEP with DMAPP, pK_a calculations, ^{1}H NMR of **4** (PDF)

AUTHOR INFORMATION

Corresponding Authors

*E-mail: matthias.witschel@basf.com.
*E-mail: markus.fischer@hsfs.org.
*E-mail: michael.groll@tum.de.
*E-mail: diederich@org.chem.ethz.ch.

ORCID

Anatol Schwab: 0000-0002-4608-1681
Markus Fischer: 0000-0001-7243-4199
Michael Groll: 0000-0002-1660-340X
François Diederich: 0000-0003-1947-6327

Author Contributions

A.S. and F.D. analyzed all data and wrote the manuscript. A.S. performed synthesis. B.I. and M.F. performed biochemical experiments. A.F., A.K., and M.G. performed crystallographic experiments. M.S. and A.B. designed experiments. M.C.W. performed greenhouse experiments. All authors have given approval to the final version of the manuscript.

Funding

We thank the ETH Research Council (Grant ETH-01 13-2) and SFB749/A10 (M.G.) for support of this work.

Notes

The authors declare no competing financial interest.

ABBREVIATIONS

G3P, glyceraldehyde-3-phosphate; DXS, 1-deoxy-D-xylulose-5-phosphate synthase (EC 2.2.1.7); IspC/DXR, 1-deoxy-D-xylulose-5-phosphate reductoisomerase (EC 1.1.1.267); IspD, 4-diphosphocytidyl-2*C*-methyl-D-erythritol synthase (EC 2.7.7.60); MEP, 2*C*-methyl-D-erythritol 4-phosphate; CTP, cytidine triphosphate; PP_i, pyrophosphate; CDP-ME, 4-diphosphocytidyl-2*C*-methyl-D-erythritol; IspE, 4-diphosphocytidyl-2*C*-methyl-D-erythritol kinase (EC 2.7.1.148); IspF, 2*C*-methyl-D-erythritol-2,4-cyclodiphosphate synthase (EC 4.6.1.12); IspG, 2*C*-methyl-D-erythritol-2,4-cyclodiphosphate reductase (EC 1.17.4.3); IspH, 1-hydroxy-2(*E*)-methylbutenyl-4-diphosphate reductase (EC 5.3.3.2); IPP, isopentenyl diphosphate; DMAPP, dimethylallyl diphosphate

REFERENCES

(1) Menne, H., and Köcher, H. (2012) HRAC classification of herbicides and resistance development, In *Modern Crop Protection Compounds*, 2nd ed. (Krämer, W., Schirmer, U., Jeschke, P., and Witschel, M., Eds.), pp 5−28, Wiley-VCH, Weinheim, Germany.

(2) Frank, A., and Groll, M. (2017) The Methylerythritol Phosphate Pathway to Isoprenoids. *Chem. Rev. 117*, 5675−5703.

(3) Eisenreich, W., Bacher, A., Arigoni, D., and Rohdich, F. (2004) Biosynthesis of isoprenoids via the non-mevalonate pathway. *Cell. Mol. Life Sci. 61*, 1401−1426.

(4) Rodríguez-Concepción, M., and Boronat, A. (2002) Elucidation of the methylerythritol phosphate pathway for isoprenoid biosynthesis in bacteria and plastids. A metabolic milestone achieved through genomics. *Plant Physiol. 130*, 1079−1089.

(5) Rohmer, M. (1999) The discovery of a mevalonate-independent pathway for isoprenoid biosynthesis in bacteria, algae and higher plants. *Nat. Prod. Rep. 16*, 565−574.

(6) Witschel, M., Röhl, F., Niggeweg, R., and Newton, T. (2013) In search of new herbicidal inhibitors of the non-mevalonate pathway. *Pest Manage. Sci. 69*, 559−563.

(7) Witschel, M. C., Höffken, H. W., Seet, M., Parra, L., Mietzner, T., Thater, F., Niggeweg, R., Röhl, F., Illarionov, B., Rohdich, F., Kaiser, J., Fischer, M., Bacher, A., and Diederich, F. (2011) Inhibitors of the herbicidal target IspD: allosteric site binding. *Angew. Chem., Int. Ed. 50*, 7931−7935.

(8) Kunfermann, A., Witschel, M., Illarionov, B., Martin, R., Rottmann, M., Höffken, H. W., Seet, M., Eisenreich, W., Knölker, H.-J., Fischer, M., Bacher, A., Groll, M., and Diederich, F. (2014) Pseudilins: halogenated, allosteric inhibitors of the non-mevalonate pathway enzyme IspD. *Angew. Chem., Int. Ed. 53*, 2235−2239.

(9) Martino-Catt, S. J., Feng, P. C. C., and Padgette, S. R. (2012) Genetically modified herbicide-resistant crops, In *Modern Crop Protection Compounds*, 2nd. ed. (Krämer, W., Schirmer, U., Jeschke, P., and Witschel, M., Eds.), pp 399−437, Wiley-VCH, Weinheim, Germany.

(10) Legeay, S., Clere, N., Hilairet, G., Do, Q.-T., Bernard, P., Quignard, J.-F., Apaire-Marchais, V., Lapied, B., and Faure, S. (2016) The insect repellent *N*,*N*-diethyl-*m*-toluamide (DEET) induces angiogenesis *via* allosteric modulation of the M3 muscarinic receptor in endothelial cells. *Sci. Rep. 6*, 28546.

(11) Changeux, J.-P. (2013) 50 years of allosteric interactions: the twists and turns of the models. *Nat. Rev. Mol. Cell Biol. 14*, 819−829.

(12) Wootten, D., Christopoulos, A., and Sexton, P. M. (2013) Emerging paradigms in GPCR allostery: implications for drug discovery. *Nat. Rev. Drug Discovery 12*, 630−644.

(13) Clough, J. M., Dale, R. P., Elsdon, B., Hawkes, T. R., Hogg, B. V., Howell, A., Kloer, D. P., Lecoq, K., McLachlan, M. M., Milnes, P. J., O'Riordan, T. J. C., Ranasinghe, S., Shanahan, S. E., Sumner, K. D., and Tayab, S. (2016) Synthesis and evaluation of hydroxyazolopyrimidines as herbicides; the generation of amitrole in planta. *Pest Manage. Sci. 72*, 2254−2272.

(14) Richard, S. B., Bowman, M. E., Kwiatkowski, W., Kang, I., Chow, C., Lillo, A. M., Cane, D. E., and Noel, J. P. (2001) Structure of 4-diphosphocytidyl-2-C-methylerythritol synthetase involved in mevalonate-independent isoprenoid biosynthesis. *Nat. Struct. Biol. 8*, 641−648.

(15) *The PyMOL molecular graphics system*, version 1.7; Schrödinger, LLC, 2015.

(16) Ho, B. K., and Gruswitz, F. (2008) HOLLOW: Generating accurate representations of channel and interior surfaces in molecular structures. *BMC Struct. Biol. 8*, 49.

(17) Bochevarov, A. D., Harder, E., Hughes, T. F., Greenwood, J. R., Braden, D. A., Philipp, D. M., Rinaldo, D., Halls, M. D., Zhang, J., and Friesner, R. A. (2013) Jaguar: A high-performance quantum chemistry software program with strengths in life and materials sciences. *Int. J. Quantum Chem. 113*, 2110−2142.

(18) Cherukupalli, S., Karpoormath, R., Chandrasekaran, B., Hampannavar, G. A., Thapliyal, N., and Palakollu, V. N. (2017) An insight on synthetic and medicinal aspects of pyrazolo[1,5-*a*] pyrimidine scaffold. *Eur. J. Med. Chem. 126*, 298−352.

(19) Burkholder, P. R., Pfister, R. M., and Leitz, F. H. (1966) Production of a Pyrrole Antibiotic by a Marine Bacterium. *Appl. Microbiol. 14*, 649−653.

(20) Andersen, R. J., Wolfe, M. S., and Faulkner, D. J. (1974) Autotoxic antibiotic production by a marine Chromobacterium. *Mar. Biol. 27*, 281−285.

(21) Pudleiner, H., and Laatsch, H. (1990) Synthese cyclischer und sterisch gehinderter Pseudiline. *Liebigs Ann. Chem. 1990*, 423−432.

(22) Martin, R., Jäger, A., Böhl, M., Richter, S., Fedorov, R., Manstein, D. J., Gutzeit, H. O., and Knölker, H.-J. (2009) Total synthesis of pentabromo- and pentachloropseudilin, and synthetic analogues-allosteric inhibitors of myosin ATPase. *Angew. Chem., Int. Ed. 48*, 8042−8046.

(23) Agarwal, V., El Gamal, A. A., Yamanaka, K., Poth, D., Kersten, R. D., Schorn, M., Allen, E. E., and Moore, B. S. (2014) Biosynthesis of polybrominated aromatic organic compounds by marine bacteria. *Nat. Chem. Biol. 10*, 640−647.

DOI: 10.1021/acschembio.7b00004
ACS Chem. Biol. XXXX, XXX, XXX−XXX

(24) Persch, E., Dumele, O., and Diederich, F. (2015) Molecular recognition in chemical and biological systems. *Angew. Chem., Int. Ed. 54*, 3290−3327.
(25) Wilcken, R., Zimmermann, M. O., Lange, A., Joerger, A. C., and Boeckler, F. M. (2013) Principles and Applications of Halogen Bonding in Medicinal Chemistry and Chemical Biology. *J. Med. Chem. 56*, 1363−1388.
(26) Cavallo, G., Metrangolo, P., Milani, R., Pilati, T., Priimagi, A., Resnati, G., and Terraneo, G. (2016) The Halogen Bond. *Chem. Rev. 116*, 2478−2601.
(27) Illarionova, V., Kaiser, J., Ostrozhenkova, E., Bacher, A., Fischer, M., Eisenreich, W., and Rohdich, F. (2006) Nonmevalonate terpene biosynthesis enzymes as antiinfective drug targets: substrate synthesis and high-throughput screening methods. *J. Org. Chem. 71*, 8824−8834.
(28) Zimmermann, M. O., Lange, A., Zahn, S., Exner, T. E., and Boeckler, F. M. (2016) Using Surface Scans for the Evaluation of Halogen Bonds toward the Side Chains of Aspartate, Asparagine, Glutamate, and Glutamine. *J. Chem. Inf. Model. 56*, 1373−1383.
(29) Salonen, L. M., Ellermann, M., and Diederich, F. (2011) Aromatic rings in chemical and biological recognition: energetics and structures. *Angew. Chem., Int. Ed. 50*, 4808−4842.
(30) Meyer, E. A., Castellano, R. K., and Diederich, F. (2003) Interactions with aromatic rings in chemical and biological recognition. *Angew. Chem., Int. Ed. 42*, 1210−1250.
(31) Harder, M., Kuhn, B., and Diederich, F. (2013) Efficient stacking on protein amide fragments. *ChemMedChem 8*, 397−404.
(32) Müller, K., Faeh, C., and Diederich, F. (2007) Fluorine in pharmaceuticals: looking beyond intuition. *Science 317*, 1881−1886.
(33) Lauber, B. S., Hardegger, L. A., Asraful, A. K., Lund, B. A., Dumele, O., Harder, M., Kuhn, B., Engh, R. A., and Diederich, F. (2016) Addressing the glycine-rich loop of protein kinases by a multifacetted interaction network: inhibition of PKA and a PKB mimic. *Chem. - Eur. J. 22*, 211−221.
(34) Gilday, L. C., Robinson, S. W., Barendt, T. A., Langton, M. J., Mullaney, B. R., and Beer, P. D. (2015) Halogen Bonding in Supramolecular Chemistry. *Chem. Rev. 115*, 7118−7195.
(35) Dumele, O., Schreib, B., Warzok, U., Trapp, N., Schalley, C. A., and Diederich, F. (2017) Halogen-Bonded Supramolecular Capsules in the Solid State, in Solution, and in the Gas Phase. *Angew. Chem., Int. Ed. 56*, 1152−1157.
(36) Hardegger, L. A., Kuhn, B., Spinnler, B., Anselm, L., Ecabert, R., Stihle, M., Gsell, B., Thoma, R., Diez, J., Benz, J., Plancher, J.-M., Hartmann, G., Banner, D. W., Haap, W., and Diederich, F. (2011) Systematic Investigation of Halogen Bonding in Protein−Ligand Interactions. *Angew. Chem., Int. Ed. 50*, 314−318.
(37) Wilcken, R., Zimmermann, M. O., Lange, A., Joerger, A. C., and Boeckler, F. M. (2013) Principles and Applications of Halogen Bonding in Medicinal Chemistry and Chemical Biology. *J. Med. Chem. 56*, 1363−1388.
(38) Gale, P. A., and Steed, J. W. (2012) *Supramolecular Chemistry: From Molecules to Nanomaterials*, Vol. 3 (Molecular recognition), Wiley, Chichester, United Kingdom.
(39) Dayan, F. E., Daga, P. R., Duke, S. O., Lee, R. M., Tranel, P. J., and Doerksen, R. J. (2010) Biochemical and structural consequences of a glycine deletion in the α-8 helix of protoporphyrinogen oxidase. *Biochim. Biophys. Acta, Proteins Proteomics 1804*, 1548−1556.
(40) Rosenstiel, T. N., Fisher, A. J., Fall, R., and Monson, R. K. (2002) Differential accumulation of dimethylallyl diphosphate in leaves and needles of isoprene- and methylbutenol-emitting and nonemitting species. *Plant Physiol. 129*, 1276−1284.
(41) Gräwert, T., Span, I., Eisenreich, W., Rohdich, F., Eppinger, J., Bacher, A., and Groll, M. (2010) Probing the reaction mechanism of IspH protein by x-ray structure analysis. *Proc. Natl. Acad. Sci. U. S. A. 107*, 1077−1081.
(42) Gabrielsen, M., Kaiser, J., Rohdich, F., Eisenreich, W., Laupitz, R., Bacher, A., Bond, C. S., and Hunter, W. N. (2006) The crystal structure of a plant 2*C*-methyl-D-erythritol 4-phosphate cytidylyltransferase exhibits a distinct quaternary structure compared to bacterial homologues and a possible role in feedback regulation for cytidine monophosphate. *FEBS J. 273*, 1065−1073.

DOI: 10.1021/acschembio.7b00004
ACS Chem. Biol. XXXX, XXX, XXX−XXX